Lunar South Pole Hydrogen & Water Ice Deposits: Constraints from Lunar Prospector magnetic field observations

Ethan W. Schaler

Magnet Program at Montgomery Blair H.S., Silver Spring, Maryland, USA

Michael E. Purucker

Raytheon at Planetary Geodynamics Laboratory, NASA/GSFC, Greenbelt, Maryland, USA

Abstract. The south polar region of the moon has long been believed to contain preserved deposits of water ice. Examinations have been performed by both neutron spectrometers and long-wave radar as a means of identifying regions that potentially contain these deposits, but doubts remain. Magnetic field measurements from the Lunar Prospector's fluxgate magnetometer were used to model the region's internal magnetic field via an equivalent source dipole technique. Magnetic fields originating from the moon can act to stand off the solar wind and prevent the implantation of solar wind hydrogen. We find a positive correlation between high hydrogen presence and an elevated magnetic field, suggesting that implanted hydrogen is not a significant hydrogen source. Six craters - Shoemaker, Nobile, and unnamed craters at (87.7° S, 99.8° W), (85.5° S, 48.1° E), (87.5° S, 4.0° W), and (88.5° S, 87.0° W) - have been isolated as likely targets for water ice deposits.

1. Introduction

The lunar south pole has long attracted attention for the proposed water ice deposits in permanently shadowed craters (aka. 'cold traps'). Despite intense scrutiny both from Earth-based telescopes and satellites - Clementine (1994) and Lunar Prospector (1998-1999) - however, definitive proof of the existence and location of such water deposits remains elusive.

Previous attempts to identify water ice deposits have involved analyses of the region with the neutron spectrometer sensor onboard the Lunar Prospector and ground-based radar devices. Results of such studies vary widely: *Feldman et al.* [2000] utilized neutron flux data to predict the mass content of water in the approximately 4000 km^2 of permanent shade near the south pole as being 2.4 x 10^8 metric tons, while analysis of long-wave radar data in *Campbell et al.* [2003] generates the conclusion that "any ice...must be in the form of disseminated grains or thin interbedded layers." Both methods have their shortcomings. Neutron spectrometer-based analyses lack the ability to definitively identify the state of the hydrogen being measured - potentially existing as a component of water or another chemical compound, or having been implanted in the lunar soil by the solar wind. Radar-imaging requires a direct line of sight with the region being analyzed (a difficult feat due to the inclination of the moon in relation to Earth) and can be confounded by features like vertical crater walls. Furthermore, this technique requires a relatively large/thick deposit of ice to produce an identifying "coherent backscatter" [*Campbell et al.*, 2003], thus regions with dispersed or little water are difficult to distinguish.

Magnetic data can provide insight into the geological composition of the region and identify major anomalies that influence the surrounding lunar system. Indeed, the presence of a strong magnetic field is capable of protecting the lunar regolith from external interference by standing off fields of non-lunar origin (solar wind). Analysis of the magnetic field reinforces analyses of the south polar region with regard to the presence and distribution of water ice deposits.

2. Data

The magnetic field data analyzed in this study was measured by the Lunar Prospector's triaxial fluxgate magnetometer - a device capable of measuring the magnetic fields (to under 0.05 nT) in three-dimensional space. For the purposes of this project, the maximum accuracy is estimated at 0.5 nT due to uncertainties (spin averaging, etc.). Level 1B data was acquired from the Planetary Data System archives. The magnetic field data was transformed from SEL coordinates into the local spherical coordinate system defined by B_r (out/in), B_θ (south/north), and B_ϕ (east/west).

Modeling of the lunar south pole's magnetic field utilized observations collected on 35 of the 560 days (Table 1) during which the magnetometer was in operation - 27 days in the magnetotail of Earth, 4 days in the magnetosheath, and 4 days in the solar wind (based on Geocentric Solar Ecliptic (GSE) coordinates). All days included in the analysis were taken after the Lunar Prospector's orbital alteration on December 19, 1998 (day 338 of the mission) which reduced the satellite's orbital altitude from 100$\pm$1 km to 33$\pm$17 km (field strength decays as the cube of the distance, so lower altitudes yield measurements of larger magnitude). These days were selected for optimal accuracy: high pass-to-pass

coherence of magnetic signatures in conjunction with strong measurements and minimal noise. The data is evenly distributed throughout the examined region ($180°W - 180°$ E, $75 - 90°$ S) and incorporates a wide range of sampling altitudes (Figure 1).

3. Model

3.1. External Magnetic Field

A simple model of the external magnetic field was developed [*Purucker et al.*, 2006] and removed from the Lunar Prospector observations. The model is motivated by the physics of the external field in quiet times, and during times when the moon is in the earth's magnetic tail. The data is partitioned into half-orbital passes centered at the poles and extending from equator-crossing to equator-crossing. A uniform external field is then determined for each half-orbit, based on a least-squares approach that utilizes the 3-dimensional vector observations. *Purucker et al.* [2006] applied this technique to half-orbits extending from pole to pole and demonstrated that in periods when the moon was in the Earth's magnetotail, there was a good correspondence between directions and intensities predicted by the T96 model [*Tsyganenko*, 1996] of the tail and the uniform external field determined from the Lunar Prospector observations. The approach outlined here differs from the filtering approach of *Hood et al.* [2001] in that it treats the removed field as a potential field.

3.2. Equivalent Source

The internal magnetic fields and sources of the lunar crust (near-surface layer) are modeled using an equal-area grid of 2530 dipoles [*Purucker et al.*, 1996; *Dyment and Arkani-Hamed*, 1998]. The magnetic dipoles are expressed in a spherical coordinate system and

defined as being radially-oriented with a 0.5° latitude spacing and variable longitude spacing. The dipoles are constrained through the use of radial (B_r), theta (B_θ), and phi (B_ϕ) magnetic field observations. Determination of these dipoles allows for the generation of altitude-normalized maps of B_r, B_θ, B_ϕ, and $\|B\|$ at 30 km altitude [*Purucker et al.*, 2000]. Root Mean Square (RMS) values of the magnetic field observations subsequent to the removal of internal and external models are as follows: $B_r = 1.38$, $B_\theta = 2.11$, $B_\phi = 2.55$, and an overall $RMS = 2.07\ nT$.

4. Analysis & Discussion

4.1. Craters of Interest

14 craters in perpetual shadow - primary regions of interest for locating water ice - were identified by *Margot et al.* [1999], *Feldman et al.* [2000], and *Berezhnoy et al.* [2005] (Figure 2A). These regions were analyzed with regard to both local magnetic field strength (at a simulated altitude of 30 km) and neutron flux (Figure 2B & C).

Shoemaker is located almost directly over a large magnetic anomaly (Figure 3) with a scalar field strength of approx. 3.24 nT at 30 km altitude and is also in a region identified as having a low neutron flux (.215 - .217 $neutrons/cm^2/sec$). Crater Unnamed 5 is located in a region with a scalar magnetic field of approx. 1.29 - 2.20 nT and a neutron flux of .215 - .217 $neutrons/cm^2/sec$. Craters Nobile and Unnamed 3 (border one-another), Unnamed 2, and Unnamed 6 all exhibit neutron fluxes of .217 - .219 $neutrons/cm^2/sec$ and a predicted scalar magnetic field between 1 - 3 nT.

The characteristics of the 6 craters discussed above are optimal for the presence/preservation of water ice deposits. Evidence pointing to the early accretion of water

ice as opposed to the long-term implantation of hydrogen is discussed below. The neutron flux measurements of epithermal neutrons are inversely related to the presence/density of hydrogen (specifically the equal-mass nucleus - a neutron); the low flux measurements correspond to a high density of hydrogen atoms - the identifying signature of a water deposit. Lack of direct sunlight produces extremely low temperatures (regions in permanent shadow are believed to have a maximum temperature not exceeding 110° K [*Berezhnoy et al.*, 2005]) that prevent/reduce the rate of sublimation. The relatively strong internal magnetic fields observed produce a mini-magnetosphere [*Kurata et al.*, 2005] that prevents both the interference of the solar wind and the implantation of hydrogen. The effectiveness and scope of this mini-magnetosphere is well documented: the data is organized spatially - sequential (adjacent) passes demonstrate a strong correlation, a characteristic demonstrating that the mini-magnetosphere's field of influence extends above the altitudes of measurement (33 ± 17 km).

Craters not referred to either exhibit weak local magnetic fields or high neutron flux observations, and thus are less likely candidates for containing deposits of water ice.

4.2. Potential Sources of Observed Hydrogen

In previous analyses, the potential presence of water ice in the south polar region has been disputed due to the inability to determine the origin/form of the 1670 ± 890 ppm hydrogen [*Feldman et al.*, 2000] observed in the lunar regolith. Competing theories include that the observed hydrogen is a component of water, a component of other compounds/minerals, or has been implanted in the lunar soil by the solar wind [*Feldman et al.*, 2000]. Results of the magnetic field analysis, however, potentially contradict the theory of

hydrogen implantation. The solar wind is composed primarily of charged particles (ionized hydrogen being the most common), which generate a magnetic field when moving. A strong magnetic field, like the one observed near the lunar south pole, is capable of repelling/diverting - standing off - the solar wind (at least during calm phases). The result is twofold: magnetically shielded regions would contain far lower quantities of solar wind-implanted hydrogen (than those measured elsewhere on the moon) and would also be protected from radiation/particle bombardment, thereby preserving any existing water deposits. It is highly likely, therefore, that the hydrogen is preserved as a component of a larger compound.

4.3. Caveats

The modeled crustal magnetization and the subsequent scalar field projection produced appears to correlate with both multiple craters containing regions of permanent darkness and the measurements of neutron flux. However, there are certain issues that must be addressed regarding the strength of these results.

Unfit Data: The south polar region contains a complex magnetic field with a rather small magnitude and has a large amount of interference from far stronger fields (Earth's magnetosphere and the solar wind). As a result, it is particularly difficult to model. This is evident with regard to the overall $RMS = 2.07\ nT$, which is relatively large considering the predominant range of the scalar magnetic field is 0 - 4 nT. Improvements to accuracy could theoretically be achieved through increased concentrations of dipoles in the model, however the dipole distribution (approx. 2° longitude separation at 75° S) is already far

denser than the measurement range of the satellite (corresponds closely to the 33±16 km altitude).

Sparse Data: Certain regions contain sparse distributions of observations because many of the passes didn't meet the quality-control criteria (pass-to-pass coherence, noise level, and observed field strength) established for selecting data. Even with the external field removed before selection of the final data set (used for generation of the equivalent source model), the data often contained considerable noise from non-lunar sources and exhibited little pass-to-pass coherence. For this reason, the region between 30 - 45° E and 75 - 90° S is particularly sparse (it also has a exceptionally strong magnetic field).

5. Conclusion

The results of this study further refine the potential location of water ice deposits at the lunar south pole. Six specific craters - Shoemaker, Nobile, and Unnamed 2, 3, 5, and 6 (Figure 2A) - have been isolated as highly likely targets for such deposits. Further analysis, including observations on the next lunar mission, the Lunar Reconnaissance Orbiter (2008), should be targeted at regions such as those identified here.

References

Berezhnoy, A., E. Kozlova, and V. Shevchenko (2005), The cold traps near the south pole of the moon, in *Lunar and Planetary Science XXXVI*, Abstract #1061, Lunar and Planetary Institute.

Campbell, B., D. Campbell, J. Chandler, A. Hine, M. Nolan, and P. Perrillat (2003), Radar imaging of the lunar poles, *Nature*, *426*(6963), 137–138.

Dyment, J., and J. Arkani-Hamed (1998), Equivalent source magnetic dipoles revisited, *Geophys. Res. Lett.*, *25*(11), 2003–2006.

Feldman, W., S. Maurice, A. Binder, B. Barraclough, R. Elphic, and D. Lawrence (1998), Fluxes of fast and epithermal neutrons from lunar prospector: Evidence for water ice at the lunar poles, *Science*, *281*(5382), 1496 – 1500.

Feldman, W., D. Lawrence, R. Elphic, B. Barraclough, S. Maurice, I. Genetay, and A. Binder (2000), Polar hydrogen deposits on the moon, *JGR-Planets*, *105*, 4175–4195.

Hood, L., A. Zakharian, J. Halekas, D. Mitchell, R. Lin, M. Acuña, and A. Binder (2001), Initial mapping and interpretation of lunar crustal magnetic anomalies using Lunar Prospector magnetometer data, *J. Geophys. Res.*, *106*, 27,825–27,839.

Kurata, M., H. Tsunakawa, Y. Saito, H. Shibuya, M. Matsushima, and H. Shimizu (2005), Mini-magnetosphere over the Reiner Gamma magnetic anomaly region on the Moon, *Geophys. Res. Lett.*, *32*, L24205, doi:10.1029/2005GL024097.

Margot, J., D. Campbell, R. Jurgens, and M. Slade (1999), Topography of the lunar poles from radar interferometry: A survey of cold trap locations, *Science*, *284*, 1658–1660.

Purucker, M., T. Sabaka, and R. Langel (1996), Conjugate gradient analysis: a new tool for studying satellite magnetic data sets, *Geophys. Res. Lett.*, *23*(5), 507–510.

Purucker, M., D. Ravat, H. Frey, T. Sabaka, and M. Acuña (2000), An altitude-normalized magnetic map of Mars and its interpretation, *GRL*, *27*(16), 2449–2452.

Purucker, M., T. Sabaka, N. Tsyganenko, N. Olsen, J. Halekas, and M. Acuña (2006), The Lunar magnetic field environment: interpretation of new maps of the internal and external fields, in *Lunar and Planetary Science XXXVII*, Abstract #1933, Lunar and

182 Planetary Institute.

183 Tsyganenko, N. (1996), Effects of the solar wind conditions on the global magnetospheric

184 configuration as deduced from data-based field models, in *European Space Agency Publ.*

185 *ESA SP-389*, pp. 181–185.

186 USGS Astrogeology Research Program (2006), Earth's moon: Clementine color-coded

187 shaded relief.

Table 1. Days (1998-1999) identified as containing high-quality data and utilized in the lunar magnetic field model.

Dec.	Jan.	Feb.	Mar.	Apr.	May	Jun.	Jul.
31	1	1	1	1	1	14	1
	3	21	2	27	2	27	3
	30		3	28	28	28	9
			30	29	29	29	10
			31	30	30	30	26
					31		27
							28
							29

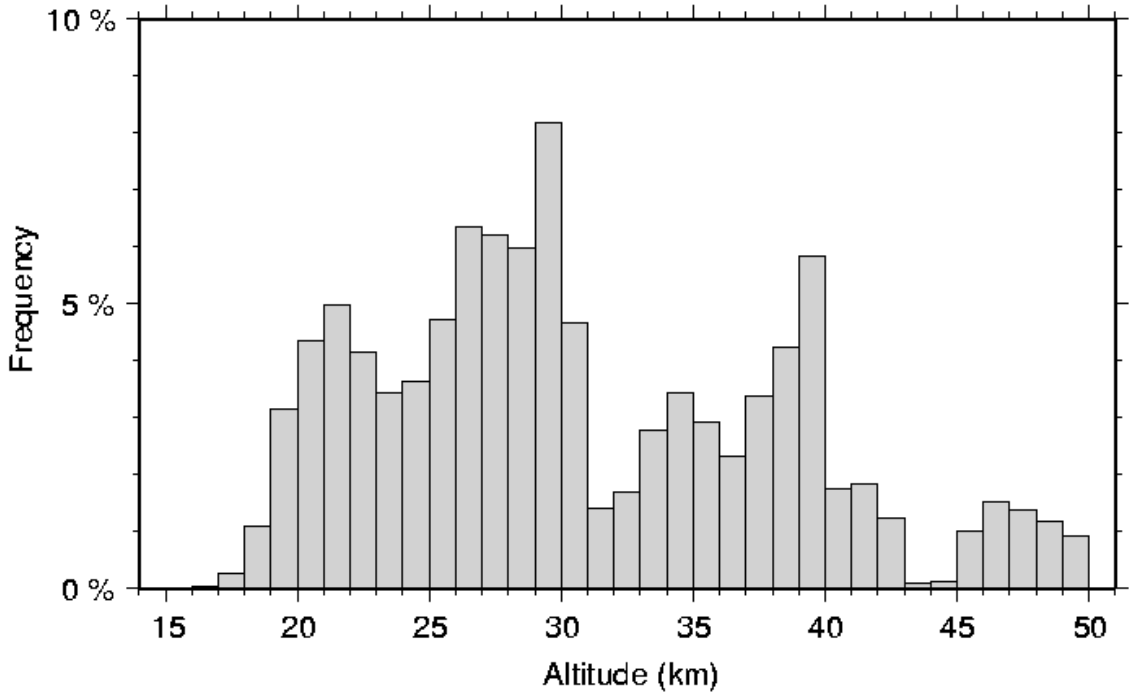

Figure 1. The distribution of altitudes in the data over the lunar south pole.

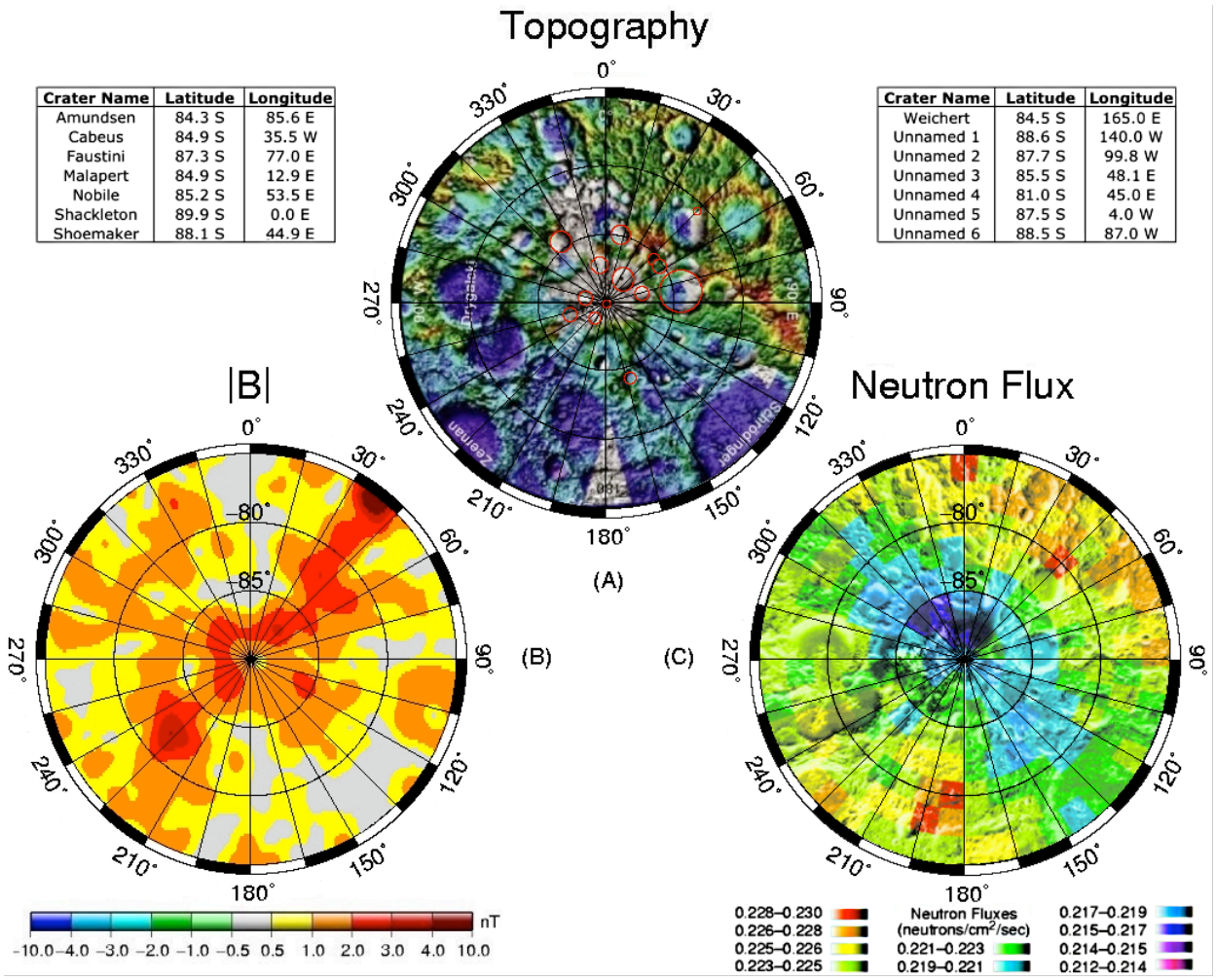

Figure 2. Comparison of three views of the south polar region (75−90° S). (A) A shaded relief topographic map of the lunar surface (modified from *USGS Astrogeology Research Program* [2006]). Craters highlighted in red represent regions found to exist in perpetual shadow (*Margot et al.* [1999], *Feldman et al.* [2000] and *Berezhnoy et al.* [2005]). (B) An altitude-normalized projection (30 *km* altitude) of the magnetic field's scalar product ($\|B\|$) as generated from an equivalent source modeling of the crustal magnetism. (C) The neutron flux (modified from *Feldman et al.* [1998]). Neutron flux is measured in terms of *epithermal neutron counts*$/cm^2/sec$ and the presence of hydrogen is inversely related to the flux analyzed here.

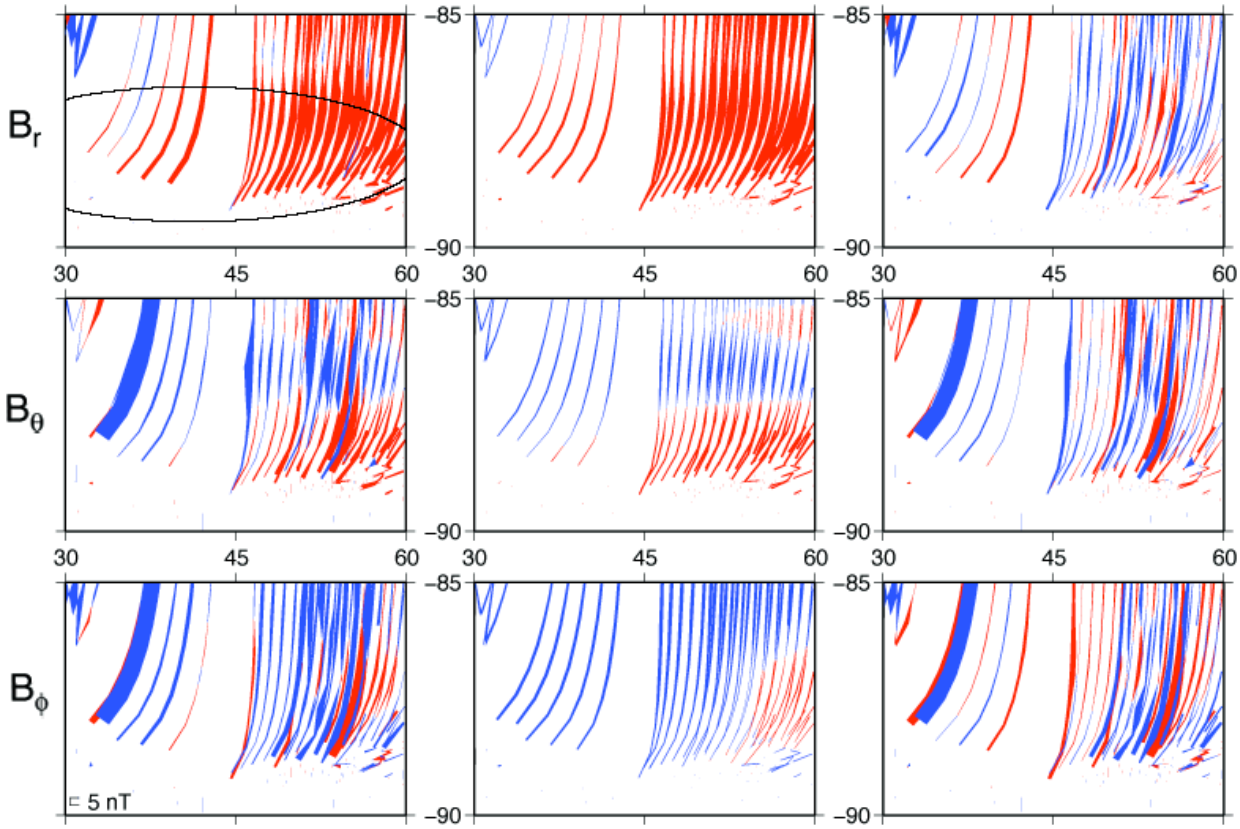

Figure 3. Magnetic profiles over the lunar south pole at crater Shoemaker, an outline of which appears in the top left box. Plots depict the observations of the magnetic field after the external field has been removed (left column), a potential function representation of the observations based on inversion of the dipole model (center column), and the residual data (right column). Magnetic field components are arranged as B_r (top row), B_θ (center row), and B_ϕ (bottom row). Red segments depict positive magnetic fields; blue segments depict negative magnetic fields.